Journal of Coastal Research	5	4	777-789	Fort Lauderdale, Florida	Fall 1989

Effects of Wave-Induced Friction on a Muddy Seabed Modelled as a Bingham-Plastic Fluid

Kofei Liu and Chiang C. Mei

Department of Civil Engineering
Massachusetts Institute of Technology
Cambridge, MA 02139

ABSTRACT

LIU, K. and Mei, C.C., 1989. Effects of wave-induced friction on a muddy seabed modelled as a Bingham-plastic fluid. *Journal of Coastal Research*, 5(4), 777-789. Fort Lauderdale (Florida). ISSN 0749-0208.

Fluid mud found at the bottom of some estuaries and coastlines contains a high concentration of clay particles. The rheological properties of this cohesive material is very complex and there have been vastly different models for predicting the mutual effects of mud and waves. In this paper we focus on the Bingham-plastic behavior known to exist in estuary and river mud with high concentration. By including interfacial friction, motion in a thin mud layer induced by a solitary wave propagating in a much thicker layer of overlying water is analyzed. Effects of the mud motion on wave damping is then calculated for both horizontal and sloping sea beds.

ADDITIONAL INDEX WORDS: *Bingham fluids, cohesive sediments, friction factor, fluid mud, solitary waves, mass transport, wave damping.*

INTRODUCTION

Depending on the clay concentration, chemical composition, and the level of shearing rate, cohesive fluid mud can have vastly different rheological behavior. When the applied stress is low, fluid mud can behave like a viscoelastic solid. On the other hand, when the stress is sufficiently high it can behave approximately like a Bingham plastic fluid. A yield stress has to be exceeded before permanent shearing can occur. In simple shear the Bingham law states that

$$\mu_m \frac{\partial u_m}{\partial y} = 0 \qquad |\tau| < \tau_0$$
$$= \tau - \tau_0 \operatorname{sgn} \frac{\partial u_m}{\partial y} \qquad |\tau| > \tau_0 \tag{1}$$

where u_m is the mud velocity, τ_0 is yield stress and μ_m the mud viscosity. Both τ_0 and μ_m increase with clay concentration. When the shearing rate is very high, mud flow becomes turbulent. The threshold of turbulence is often expressed in terms of an effective Reynolds number Re^e defined for free surface flow by many previous authors (*e.g.*, WAN, 1982) to be

$$\frac{1}{Re^e} = \frac{1}{Re^\mu} + \frac{1}{Re^\tau} \tag{2}$$

88043 received 13 June 1988; accepted in revision 7 October 1988.

where

$$Re^\mu = 4\rho_m u_m h/\mu_m \text{ and } Re^\tau = 8\rho_m u_m^2/\tau_0 \tag{3}$$

and u_m is the depth-averaged mud velocity. Thus Re^e accounts for both mud viscosity and yield stress. The rough criterion for transition from laminar to turbulent flow is

$$Re^e > 2000 \sim 3000 \tag{4}$$

Because of salinity, in estuarine mud, τ_0 can be quite appreciable and the magnitude of μ_m can be 1000 to 10000 times that of pure water (ALLERSMA, 1982). Therefore mud flow can remain laminar under many (though not all) conditions common for surface gravity waves. In another paper, MEI and LIU (1987) presented a theory of long waves over a thin mud layer on the bed of much deeper water layer, on the basis of the laminar constitutive model. Although turbulent shear stress at the interface was allowed, it was assumed to be much smaller than the yield stress. As a consequence, the dynamic pressure gradient from the wave provided the dominant driving force. A condition for this omission is that the surface wave slope must not be too small (no less than 0.1, say).

In the present paper we shall remove this restriction and consider the case where the

interfacial stress and pressure gradient are comparable. Specifically their roles in the propagation of a solitary wave in a water layer over a muddy bottom is studied. Although measurements on periodic waves over a cohesive mud layer have been reported by MAA and MEHTA (1987), SCHUCKMAN and YAMAMOTO (1982), TUBMAN and SUHAYDA (1978), information on the mud properties is unfortunately insufficient for quantitative comparison with the present theory.

FORMULATION

We follow the formulation of our earlier paper and consider two layers of superposed fluids. The top layer is clear water of mean depth H practically free of clay suspensions. The bottom layer is a fluid mud of uniform properties and has the depth h.

In the water layer, a long solitary wave of characteristic wavelength 1/k and amplitude A passes by. Assuming small amplitudes, we invoke mass conservation, to the leading order in wave slope,

$$\frac{\partial}{\partial t}(\xi - \eta) + H\frac{\partial U}{\partial x} = 0 \tag{5}$$

where U is the depth-averaged horizontal velocity, ξ is the vertical displacement of the free surface measured from the mean at y = H, and η the interface displacement from y = 0. Conservation of momentum in the top layer requires that

$$\rho\frac{\partial U}{\partial t} = -\frac{\partial p}{\partial x} - \frac{\tau_I}{H} \tag{6}$$

where p is the dynamic pressure and τ_I the interfacial stress. Conservation of vertical momentum implies that the pressure is approximately hydrostatic

$$p = \rho g(\xi - y + H) \tag{7}$$

These equations are valid only over a few wave lengths within which nonlinearity and frequency dispersion are not important.

Within the mud layer, continuity requires that

$$\rho_m\left[\frac{\partial \eta}{\partial t} + h\frac{\partial U_m}{\partial x}\right] = \epsilon + \mathcal{D} \tag{8}$$

where U_m is the depth-averaged mud velocity. ϵ and $\mathcal{D}$ are, respectively, the rates of erosion and deposition. Earlier authors have suggested empirical relations as follows:

$$\epsilon = M\left(\frac{|\tau_I|}{\tau_e} - 1\right) H(|\tau_I| - \tau_e) \tag{9}$$

where τ_e is the threshold stress which must be exceeded by $|\tau_I|$ for erosion to take place and H is the Heaviside step function, and

$$\mathcal{D} = \rho c W\left(\frac{|\tau_I|}{\tau_d} - 1\right) H(\tau_d - |\tau_I|) \tag{10}$$

where τ_d is the threshold stress below which $|\tau_I|$ must fall for deposition to occur. The lower case c and ρ are respectively the clay concentration in, and the density of, water just above the interface, and W is the effective fall velocity of the clay aggregates. These empirical relations are often used in numerical models to predict mass transport of suspended cohesive sediments in tidal flows. Let us first estimate their importance on the time and spatial scales of wind waves, by examining the following ratios which represent the righthand side of (8) to a typical term on the left-hand side,

$$\frac{\epsilon}{\rho_m h\frac{\partial U_m}{\partial x}} \sim \frac{M}{\rho_m kh\frac{A}{H}\sqrt{gH}} = \frac{M}{\rho_m \omega A\frac{h}{H}} = m \tag{11}$$

$$\frac{\mathcal{D}}{\rho_m h\frac{\partial U}{\partial x}} \sim \frac{cW}{kh\frac{A}{H}\sqrt{gH}} = \frac{cW}{\omega A\frac{h}{H}} = n$$

The order-estimates of the denominators are those associated with shallow water waves (see (38)). M ranges from 10^{-2} to 10^{-5} g cm^{-2} min^{-1} (ARIATHURAI and ARULANANDAN, 1978; PARCHURE and MEHTA, 1985). Using some typical values

$$\omega = 2\pi/10 \text{ sec}^{-1}$$
$$A = 10 \text{ cm}$$
$$M = 10^{-2} \text{g cm}^{-2}\text{min}^{-1}$$
$$c = 10^{-3}$$
$$W = 10^{-2}\text{cm sec}^{-1}$$
$$h/H = 1/10$$

we find

$$m = 2.7 \times 10^{-5} \qquad n = 1.6 \times 10^{-4}$$

Therefore, local erosion and deposition rates are usually too small to affect the wind-wave

induced motion in the mud layer, at the leading order. Indeed a sharp interface is usually present in laboratory simulation of such motions (VAN RIJN, 1985). It must be stressed that the situation is quite different in tidal flows where ω is of the order 10^{-5} sec^{-1}. The above factors m and n are then important and so are erosion and deposition. In this study (8) can be simplified to

$$\frac{\partial \eta}{\partial t} + h \frac{\partial U_m}{\partial x} \cong 0 \tag{12}$$

which can be used to calculate η from U_m.

The momentum equation in the mud layer reads

$$\rho_m \frac{\partial u_m}{\partial t} = - \frac{\partial p_m}{\partial x} + \frac{\partial \tau}{\partial y} \tag{13}$$

where the pressure is also hydrostatic

$$p_m = \rho_m g (\eta - y) + p (x, \eta, t) \tag{14}$$

We assume the mud flow to be laminar and adopt the Bingham law (1). Two distinct flow zones are then expected. Because the solitary wave acts on the mud layer only for a finite duration, the high viscosity implies that shear flow can only exist in boundary layers of the thickness of the order of magnitude $O(\delta_m)$ where

$$\delta_m = \sqrt{\mu_m/\omega\rho_m} \tag{15}$$

and $2\pi/\omega$ is the time scale of the wave. δ_m is at most a few centimeters for wind waves and usually much less than the mud layer depth. These boundary layers can be either on the interface if $\tau_I > \tau_o$ or on the bottom if $\tau > \tau_o$. Between these boundary layers the shear strain vanishes, hence there must be a plug flow where $U_m = u_p$ is constant in y. Averaging (13) vertically throughout the plug flow depth, the momentum equation for the plug flow can be written

$$\rho_m \frac{\partial u_p}{\partial t} = - \frac{\partial p_m}{\partial x} + \frac{\tau_T - \tau_0 \operatorname{sgn} u_p}{h} \tag{16}$$

the shear stress at the top of the plug flow, denoted here by τ_T, depends on the magnitude of τ_I as follows.

Case i) $\tau_I < \tau_o$. In this case there is no mud shear layer at the interface, though erosion may exist. Here we should have

$$\tau_T = \tau_I \tag{17}$$

Furthermore, we shall adopt the quadratic law for τ_I

$$\tau_I = \frac{1}{2} f\rho (U - u_p) |U - u_p| \tag{18}$$

where f is the friction factor, to be discussed further later.

Case ii) $\tau_o < \tau_I$. Now there is a thin shear layer near the top of the fluid mud. With little erosion, as discussed before, the interface is likely to be smooth so in the water above there should be a laminar sublayer immersed in a layer of constant total stress. Continuity of shear stress across the interface requires that

$$\tau_0 \operatorname{sgn} \frac{\partial u_m}{\partial y} + \mu_m \frac{\partial u_m}{\partial y} = \mu \frac{\partial u}{\partial y} \qquad y = 0 \tag{19}$$

where the right hand side represents the total water stress. In order of magnitude the above equation implies

$$O(\tau_0) + O\left(\frac{\mu_m}{\delta_m}(u_I - u_p)\right) \sim O\left(\frac{\mu}{\delta}(U - u_I)\right) \tag{20}$$

where u_I is the interface velocity and δ is the boundary layer thickness in water $\sim\sqrt{2\nu/\omega}$. Since the two terms on the left are of the same sign, it follows that

$$\frac{u_I - u_p}{U - u_I} \leq O\left(\frac{\mu}{\mu_m}\frac{\delta_m}{\delta}\right) \sim \left(\frac{\mu}{\mu_m}\right)^{1/2} \tag{21}$$

The last term is of the order 10^{-1} to 10^{-2} for fluid mud of high concentration. Therefore the velocity difference in the top shear layer is small. As a first approximation we shall ignore this difference. Consequently the interfacial stress τ_I can still be represented approximately by (18). However, the stress at the bottom of this shear layer, *i.e.*, at the top of the plug flow, must now be given by

$$\tau_T = \tau_0 \operatorname{sgn} (U - u_p) \quad \tau_I > \tau_0 \tag{22}$$

due to the Bingham behavior.

In summary, the shear stress at the top of the plug flow layer is

$$\tau_T = \tau_I = \frac{1}{2} f\rho (U - u_p)^2 \operatorname{sgn} (U - u_p), \quad \tau_I < \tau_0 \tag{23}$$

$$\tau_T = \tau_0 \operatorname{sgn} (U - u_p), \quad \tau_I > \tau_0 \tag{24}$$

Now we make use of the assumption that h/H $<<$ 1. The first consequence is that the interface displacement is negligibly small,

$$\frac{\eta}{\xi} \sim \frac{h}{H} << 1 \tag{25}$$

so that

$$p_m \sim p \tag{26}$$

The second consequence is that

$$\frac{\tau_I}{H} << \frac{\tau_I}{h} \tag{27}$$

so that the interfacial stress is much more important to mud than to the water layer. The momentum equation is now reduced to

$$\rho \frac{\partial U}{\partial t} = -\frac{\partial p}{\partial x} = \rho g \frac{\partial \xi}{\partial x} \tag{28}$$

in the water layer and

$$\rho_m \frac{\partial u_p}{\partial t} = \rho \frac{\partial U}{\partial t} + \frac{1}{h}(\tau_T - \tau_0 \operatorname{sgn} u_p) \tag{29}$$

in the plug flow with τ_T given by (23) or (24). Thus the simplifications (25) and (27) enable us to find the water wave motion in advance of the mud motion. The pressure gradient in the former drives the latter.

Finally, let u_b denote the mud velocity in the shear layer near the bottom, then

$$\rho_m \frac{\partial u_b}{\partial t} = \rho \frac{\partial U}{\partial t} + \mu_m \frac{\partial^2 u_b}{\partial y^2} \quad 0 < y + h < y_0 \tag{30}$$

At the edge of the shear flow $y+h = y_o$, where $|\tau| = \tau_o$ velocities and stresses must be continuous,

$$u_b = u_p \qquad y + h = y_0 \tag{31}$$

$$\frac{\partial u_b}{\partial y} = 0 \tag{32}$$

At the bottom there is no slip,

$$u_b = 0 \quad y + h = 0 \tag{33}$$

In this paper we only consider a solitary wave of amplitude A. In physical variables the free surface displacement is

$$\xi = A \operatorname{sech}^2 \frac{1}{2}\left(\frac{3A}{H^3}\right)^{1/2} (x - Ct) \tag{34}$$

where

$$C = [g(H + A)]^{1/2} \cong (gH)^{1/2} \tag{35}$$

The corresponding water velocity is

$$U = g\xi / C \tag{36}$$

Note that this solution is the result of a weakly nonlinear theory. However within a wave length, nonlinearity is ineffective, so that the linearized approximation of (35) is consistent with (5) and (28).

Let the wave number be defined by

$$k = \frac{1}{2}\left(\frac{3A}{H^3}\right)^{1/2} \tag{37}$$

and the following normalization be introduced:

$$\bar{x} = kx, \bar{t} = \omega t = kCt, \bar{y} = (y + h)/\delta_m \tag{38}$$

$$\bar{y}_0 = y_0/\delta_m, (\bar{U}, \bar{u}_p, \bar{u}_b) = \frac{gA}{C}(U, u_p, u_b)$$

The mud momentum equation (29) becomes

$$\frac{\partial \bar{u}_p}{\partial \bar{t}} = \frac{1}{s}\frac{\partial \bar{U}}{\partial t} + \alpha\left[\bar{\tau}_T \operatorname{sgn}(\bar{U} - \bar{u}_p) - \operatorname{sgn}(\bar{u}_p)\right] \tag{39}$$

with

$$s = \rho_m/\rho \tag{40}$$

$$\bar{\tau}_T = \begin{cases} \beta(\bar{U} - \bar{u}_p)^2 & \text{if } \beta(\bar{U} - \bar{u}_p)^2 \lesssim 1 \\ 1 & \end{cases} \tag{41}$$

The dimensionless parameter

$$\alpha = \frac{H\tau_0}{\rho_m \omega C A h} = \frac{2}{\sqrt{3}} \frac{\tau_0}{\rho_m g h}\left(\frac{H}{A}\right)^{3/2} \tag{42}$$

represents the effect of yield stress, and

$$\beta = \left(\frac{1}{\alpha s}\right)\frac{f}{2}\frac{A}{h}\frac{1}{kH} = \left(\frac{1}{\alpha s}\right)\frac{f}{h}\left(\frac{AH}{3}\right)^{1/2} \tag{43}$$

is the ratio between interfacial shear and yield stress. For later discussion of physics, it is more convenient to focus on the effect of interfacial shear alone by using the parameter

$$\frac{\beta}{\gamma} \alpha s \beta = \frac{f}{2}\frac{A}{h}\frac{1}{kH} = \frac{f}{h}\left(\frac{AH}{3}\right)^{1/2} \tag{44}$$

To have a preliminary idea of the magnitude of these parameters, we take the sample values

$$A = O(h) = 50 \text{ cm} \quad H = 10\text{m} \quad f = 0.02$$
$$\tau_o = 100 \text{ dynes cm}^{-2} \quad s = 1.1$$

then $\alpha = 0.19$, $\gamma = 0.06$ and $\beta = 0.30$. As will be found soon, f lies between 0.01 and 0.1 so that the value $f = 0.02$ just used is typical.

The friction factor f has not been measured for water/mud interface under oscillatory flow, so it can only be estimated by extrapolation of known experiments for a rough stationary bed. JONSSON (1965) has found for a fixed bed an empirical relation between f, bed roughness and the wave Reynolds number Re′ defined as $Re' = U_{max}A / \nu$. Here U_{max} is the maximum amplitude of the horizontal water velocity, A is the half orbital amplitude near the bed, and ν the kinematic viscosity of water, ($0.01 \text{ cm}^2\text{sec}^{-1}$). Since the mud/water interface is, in our exploratory experiments, smooth, we take f to be a function of the Reynolds number only.[1] In the absence of direct experiments, we propose to modify Jonsson's formula by replacing U_{max} with $U_{max} - u_{p,max}$ and changing the Reynolds number Re′ to

$$Re'' = \frac{(U_{max} - u_{p,max})A}{\nu} \tag{45}$$

Thus for a smooth interface, f is given by

$$f = \frac{2}{\sqrt{Re''}} \quad \text{if } Re'' < Re''_c \text{ (laminar)} \tag{46}$$

and

$$\frac{1}{4\sqrt{f}} + 2 \log \frac{1}{4\sqrt{f}} = \log Re'' - 1.55$$
$$\text{if } Re'' > Re''_c \text{ (turbulent)} \tag{47}$$

The critical Reynolds number Re_c' is about 20,000. As Re″ decreases, f increases from (46) and (47). Since $u_{p,max}$ is contained in Re″ by definition, f is unknown before u_p is solved.

The whole problem depends on three parameters: α, Re′ and $(1/h)\sqrt{AH/3}$ or equivalently: α, f and $(1/h)\sqrt{AH/3}$. Note that γ includes f and $(1/h)\sqrt{AH/3}$ via (44).

If we assume a trial value for f, β and γ can be obtained from (43) and (44) for a given α. We now need to compute u_p in order to find the correct f by iteration. The procedure for calculating u_p is described in the next section in terms of the two parameters α and β which appear in (39) and (41). All the overhead bars will be dropped for brevity.

[1] *For steady flows over cohesive sediments, DIXIT, MEHTA and PARTHENIADES (1982) have found experimentally that the interface is smooth.*

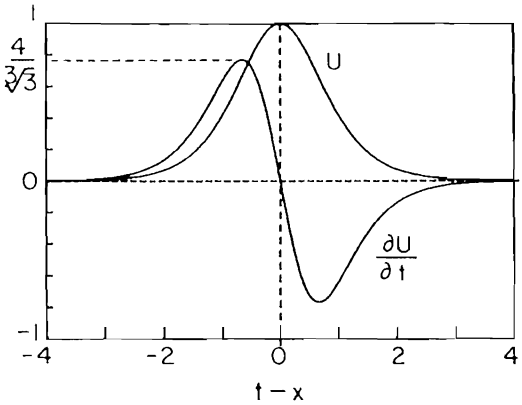

Figure 1. Time variation of U and ∂U/∂t for a solitary wave.

INITIATION AND DEVELOPMENT OF PLUG FLOW

Ignoring interfacial erosion which is important only to the suspended sediments, and the shear flow in the mud boundary layer near the interface, we now examine the plug flow in most of the mud layer under a solitary wave. The dimensionless water velocity is

$$U = \text{sech}^2(x - t) \tag{48}$$

Its direction is always forward (positive x), and its peak value is unity at $x = t$, as plotted in Fig. 1. Since the normalized stress τ_T at the top cannot exceed 1, according to (41), the plug flow cannot be initiated by the interfacial stress τ_I alone; the presence of the pressure gradient $-\partial p/\partial x = \partial U/\partial t$ is essential. Therefore the plug flow velocity u_p is expected to be in the same direction as $\partial U/\partial t$ at the start. We also plot the pressure gradient $\partial U/\partial t$ in Figure 1. Note that the maximum value is $4/3\sqrt{3}$. At the instant when the plug flow starts from rest, we have

$$0 = \frac{1}{s}\frac{\partial U}{\partial t} + \alpha(\tau_T - \text{sgn}\frac{\partial U}{\partial t}) \tag{49}$$

since $u_p = \partial u_p / \partial t = 0$. Now consider the first starting time $t_1 < 0$ at which $\partial U / \partial t > 0$. The above equation becomes

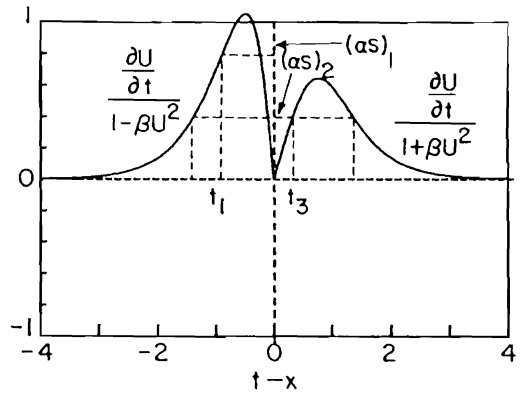

Figure 2. Criterion for the start of plug flow, $\beta = 0.5$.

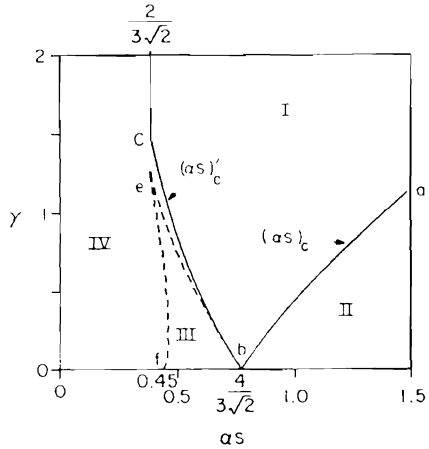

Figure 3. Dependence of the threshold yield stress parameter αs on the interfacial stress parameter γ for plug flow.
$(\alpha s)_c$: first start for forward motion,
$(\alpha s)_c$: second start for backward motion,
I: regime of continuous forward motion,
II: regime of no mud motion,
III: regime of intermittent motion,
IV: regime of continuous forward and backward motion.

$$0 = \frac{1}{s}\frac{\partial U}{\partial t} + \alpha(\tau_T - 1) \tag{50}$$

Let us distinguish two cases according to the magnitude of β defined in (43).

a) $\beta < 1$:

Since U is no greater than unity, $\beta U^2 < 1$ always and Eq. (50) becomes

$$0 = \frac{1}{s}\frac{\partial U}{\partial t} + \alpha(\beta U^2 - 1) \tag{51}$$

or

$$\alpha s = \frac{\partial U/\partial t}{1 - \beta U^2} \tag{52}$$

The right hand side is plotted on the left half of Figure 2. Only if αs is below the peak, forward plug flow can commence. The threshold value $(\alpha s)_c$ is a function of β and can be obtained numerically; the results are shown in Figure 3 which is plotted for $(\alpha s)_c$ vs $\gamma = (\alpha s)_c\beta$. When $\gamma = 0$, the interfacial stress vanishes. The maximum pressure gradient $\partial U/\partial t = 4/3\sqrt{3}$ must exceed $(\alpha s)_c$ for mud to move. Hence $(\alpha s)_c = 4/3\sqrt{3}$ for $\gamma = 0$. As the interfacial stress increases (γ increases), the mud layer can be mobilized more easily. Only by increasing the yield stress, the mud layer can remain motionless. Thus $(\alpha s)_c$ increases as γ increases as shown by curve a–b in Figure 3. To the right of a–b, no mud motion is possible. After the start, the plug flow is easily calculated by numerically integrating (39). It then goes through a peak and diminishes as the pressure gradient $\partial U/\partial t$ drops to zero at $t = 0$. It may stop at some instant t_2 on eithr side of $t = 0$. Now consider the second start t_3 of the plug flow in the backward direction. Equation (50) becomes

$$0 = \frac{1\partial U}{s\,\partial t} + \alpha(\beta U^2 + 1) \tag{53}$$

or

$$\alpha s = \frac{\left|\frac{\partial U}{\partial t}\right|}{1 + \beta U^2} \tag{54}$$

The right hand side of (53) is plotted in the right half of Figure 2; it has a lower peak. Therefore if $\alpha s = (\alpha s)_1$ which exceeds this low peak as shown in Figure 2, there can be no backward flow. But for a lower $\alpha s = (\alpha s)_2$ backward flow can be initiated. The threshold value $(\alpha s)_c'$ is plotted as a function of γ in Figure 3 as curve b–c–d.

Now the interfacial stress opposes the backward mud motion, hence is in the same direction as the threshold stress at $y = y_c$. We need less $(\alpha s)_c$ to prevent back flow to start. Thus

$(\alpha s)_c'$ decreases when γ increases as the curve b–c–d in Figure 3. If the interfacial stress exceeds the yield stress ($|\tau_I| < \tau_o$), a shear layer appears at the interface. The effect of the interfacial stress to the plug flow region becomes a constant τ_o at the top. This is why in Figure 3, $(\alpha s)_c'$ remains constant after point c as γ increases further. Quantitatively, for $|\tau_I| > \tau_o$, *i.e.*, $\beta U^2 > 1$ we have $\tau_T = 1$ from (41). Hence we replace βU^2 by 1 in (54), resulting in $(\alpha s)_c' = \max (1/2\ \partial U/\partial t) = 2/3\sqrt{3}$ as marked in Figure 3. Note that if $\beta = 1$, $\beta U^2 = 1$ only at $t = 0$, while $\partial U/\partial t = 0$. The maximum of $\frac{\partial U/\partial t}{(1 + \beta U^2)}$ must occur at time $\beta U^2 < 1$. $(\alpha s)_c' = 2/3\sqrt{3}$ can occur only for large β such that when $|\partial U/\partial t| = |\partial U/\partial t|_{max} = 4/3\sqrt{3}$, $U^2 = 1/\beta < 1$. This is why $(\alpha s)_c \to 2/3\sqrt{3}$ at a value of $\gamma \cong 1.5$. In Figure 3, there is no backward mud motion in between curves a–b and b–c–d.

b) $\beta > 1$:

Consider the first start $t_1 < 0$. Equation (52) still applies. The right hand side becomes infinite as U^2 increases from 0 to $1/\beta$ in time. Therefore for sufficiently strong interfacial shear, forward plug flow can be started at any αs by the pressure gradient from the water layer above. Let us suppose that the forward flow stops some time around $t = 0$. Backward flow begins at the instant t_3, which is the root of

$$0 = \frac{1}{s}\frac{\partial U}{\partial t} + 2\alpha \qquad t = t_3 < 0 \qquad (55)$$

For $\beta U^2 < 1$, Eq. (54) still applies. Now $\beta U^2 > 1$ is possible. When this happens $\tau_T = 1$ and (54) must be replaced by

$$\alpha s = \frac{1}{2}\left|\frac{\partial U}{\partial t}\right| \qquad \text{at } t = t_3 \qquad \text{with } (t_3 - x) > 0 \qquad (56)$$

The right hand sides of (54) and (56) are plotted for two values of β in Figs. 4.a and 4.b as functions of t–x. Since at $t-x \approx 0$, $U \approx 1$, we have

$$\frac{\left|\frac{\partial U}{\partial t}\right|}{1 + \beta U^2} = \frac{\left|\frac{\partial U}{\partial t}\right|}{1 + \beta} < \frac{1}{2}\left|\frac{\partial U}{\partial t}\right| \qquad (57)$$

and at $t-x = \infty$

$$\frac{\left|\frac{\partial U}{\partial t}\right|}{1 + \beta U^2} = \left|\frac{\partial U}{\partial t}\right| > \frac{1}{2}\left|\frac{\partial U}{\partial t}\right| \qquad (58)$$

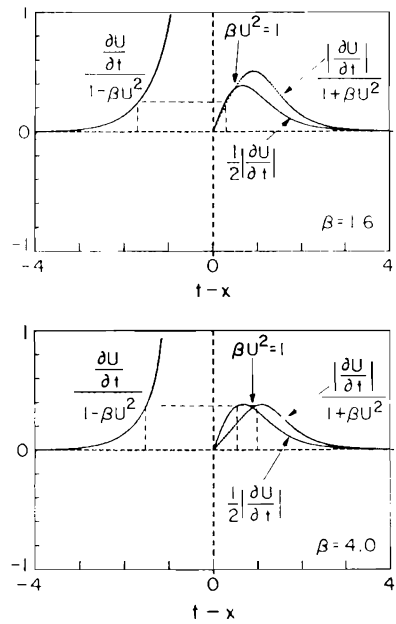

Figure 4. Criterion for the start of plug flow.
(4.a): $\beta = 1.6$ (4.b): $\beta = 4.0$

The two curves described by (54) and (56) must intersect at $\beta U^2 = 1$. There are two possibilities. Case i: $\beta U^2 = 1$ occurs for relatively small t to the left of the peak of $1/2|\partial U/\partial t|$, as shown in Figure 4.a for $\beta = 1.6$. For any αs lower than the peak of $1/2|\partial U/\partial t|$, backward flow can start. Case ii: $\beta U^2 = 1$ happens for relatively large t to the right of the peak of $1/2|\partial U/\partial t|$ as shown in Figure 4.b for $\beta = 4$. Backward flow can start twice if αs lies below both peaks and above the point $\beta U^2 = 1$.

After knowing the starting instant, u_p can be numerically integrated from (39). In Figure 5 some calculated plug flow velocities u_p are plotted. For a fixed γ, increasing αs decreases the duration as well as the amplitude of mud motion. Figure 5.b, αs is kept fixed by γ varies. For small enough αs the plug flow velocity is first forward then backward, and can be intermittent as in the cases with $\gamma = 0.01$ and 0.3. As γ increases, the greater interfacial friction, which is always forward, prolongs the forward motion in mud, and shortens the backward motion.

In the α, γ plane, the region of intermittent mud motion is inside the dashed triangle b–e–

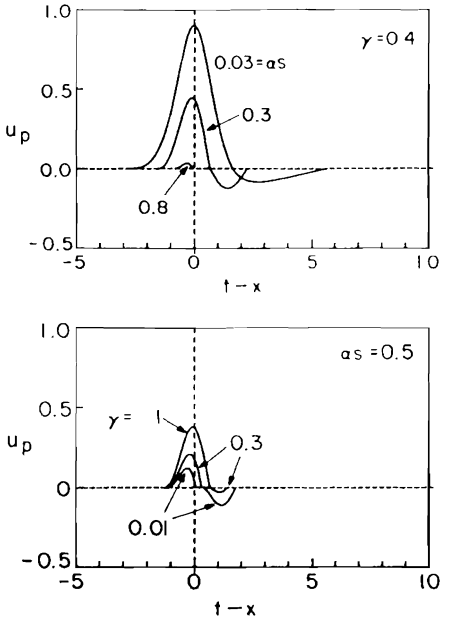

Figure 5. Sample variation of plug flow velocity u_p in time.
(5.a) $\gamma = 0.4$; $\alpha s = 0.03, 0.3, 0.8$.
(5.b) $\alpha s = 0.5$; $\gamma = 0.01, 0.3$ (intermittent), 1.0 (continuous).

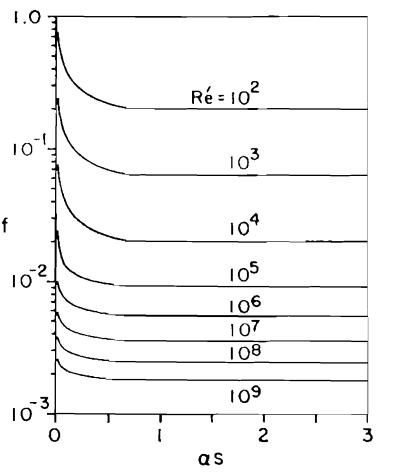

Figure 6a. Variation of f.
(6.a) f vs αs for various Re′ and $1/h\sqrt{AH/3}$ = 0.01, 0.1, 5.0.

f. For $\gamma = 0$, as predicted previously by MEI and LIU (1987) there is intermittent mud motion for $0.437 \leq \alpha s \leq 0.77$ and no motion for $\alpha s \geq 0.77$. As γ increases, the region of intermittent motion shrinks. To the left of curve a–b and outside the dashed triangle b–e–f the mud motion is continuous. Note that the region between curves a–b and b–c–d corresponds to continuous but forward mud motion only. From numerical computations we observe that for intermittent motion with $\alpha s \leq 0.437$ and $\gamma > 1$, we fall into the situation described in Figure 4.b. Mud motion stops after the first peak and starts before the second peak.

Again u_p is integrated numerically from (39); the variation of u_p with respect to α and γ is now known. We can use $u_{p,max}$ to compute f.

The friction factor can in principle be calculated by iteration for any set (α, Re′, $(1/h)\sqrt{AH/3}$). The steps are as follows. We prescribe first αs and $(1/h)\sqrt{AH/3}$. With an estimated f we get γ from (2.40). The values of αs and γ are used to calculate u_p from (39) and (41). From the calculated $u_{p,max}$, Re″ is found from (45). The new friction factor then follows from (46) or (47), and is used for the next iteration until convergence is achieved. To save computations, we choose a number of values for α, Re′ and $(1/h)\sqrt{AH/3}$ and find f through the iteration process. Interpolation is then performed to obtain f for any other intermediate values of α, Re′ and $(1/h)\sqrt{AH/3}$ without iteration. Indeed for the new parameters, f so calculated is used to obtain u_p.

Figure 6.a shows the variation of f vs αs for a wide range of Re′ and three values of $(1/h)\sqrt{AH/3}$: 0.01, 1.0 and 5.0. For large enough αs, there is no mud motion. Re′ = Re″ and f is a constant. For smaller αs, $u_{p,max}$ becomes larger and Re″ decreases for a given Re′, so f increases, according to (45) and (46). In these computations the results are much the same for all values of $(1/h)\sqrt{AH/3}$. Differences appear for much smaller Re′.

Figure 6.b shows f vs Re″ for $(1/h)\sqrt{AH/3}$ = 0.01, 1.0 and 5.0. In the case $\alpha s > 0.62$, mud does not move, so that the interface is stationary. We recover the curve for smooth turbulence in Jonsson's wave friction factor diagram. For decreasing αs, $u_{p,max}$ increases and Re″ decreases, giving rise to a larger f. Again the results are practically independent of $(1/h)\sqrt{AH/3}$.

In nature, we may estimate Re′ to lie between 10^3 and 10^6 and $(1/h)\sqrt{AH/3}$ between 10^{-2} to

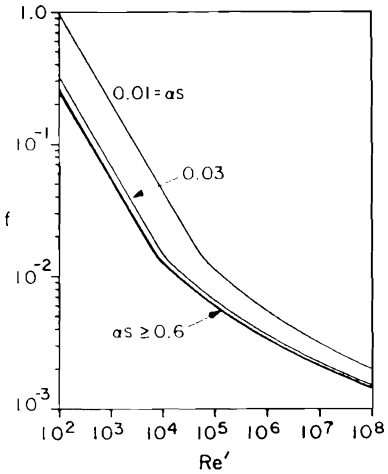

Figure 6b. Variation of f.
(6.b) f vs Re' for αs = 0.01, 0.3, 0.6 (and higher) and (1/h) $\sqrt{AH/3}$ = 0.01, 0.1, 5.0

10.0. Since in these ranges the effect of (1/h)$\sqrt{AH/3}$is hardly noticeable, we conclude that this ratio is not important in the present problem. It does not, of course, mean that each factor in this ratio is unimportant separately.

From the calculated u_p the first order volume flux per unit depth of the plug flow can be readily found

$$V_p = \int_{-\infty}^{\infty} u_p \, dt \tag{59}$$

Note that the implied scale of V_p is gA/kC^2 so that, in physical scales, the total flux in the plug flow is $(gAh/kC^2)V_p$. V_p is plotted as a function of αs in Figure 7. In the limit of αs = 0, the mud layer is not different from the clear water layer above, hence $u_p = U$ and $V_p = 2$. As the yield stress increases, V_p decreases in general with αs, except for very small γ when V_p can actually be negative. For γ > 0.0831, V_p is always positive. From (43), γ > 0.0831 corresponds to $h/H \leq f/0.144\,(A/H)^{1/2}$. It is possible that the neglected higher order effects may alter this result. As γ increases V_p increases monotonically. The flux in the shear flow layer is discussed later.

THE BOTTOM SHEAR LAYER

The shear layer at the bottom is a major contributor to energy dissipation in the mud flow.

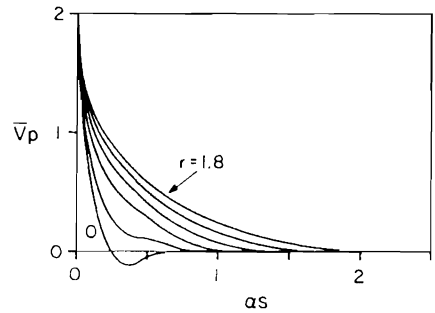

Figure 7. Total volume transport of fluid mud by plug flow $V_p = (gAh/KC^2)\,\bar{V}_p$ vs αs for various γ. From left to right γ = 0.0, 0.2, 0.6, 1.0, 1.4, 1.8.

Since its depth is expected to be small it is expedient to employ the approximate momentum integral method. Assuming the following polynomial velocity profile,

$$u_m = u_b = u_p\left[\frac{2y}{y_o} - \left(\frac{y}{y_o}\right)^2\right] \tag{60}$$

we obtain from the vertically integrated momentum equation (MEI and LIU, 1987).

$$u_p\frac{\partial y_o^2}{\partial t} + \left(\frac{6}{s}\frac{\partial U}{\partial t} - 4\frac{\partial U_p}{\partial t}\right)y_o^2 = 12u_p \tag{61}$$

This is a first order differential equation for y_o once u_p is known. Typical numerical results for the shear flow depth are presented in Figure 8. For large enough β or small enough αs, y_o becomes unbounded when u_p vanishes. By integrating (60) from 0 to y_o the flux in the shear layer is found to be $2u_py_o/3$ which is plotted in Figure 9. Although y_o is singular, u_p vanishes sufficiently fast so that the flux through the shear layer vanishes in the limit. Thus the singularity has little dynamical significance. The integrated flux is

$$V_h = \int_{-\infty}^{\infty} dt\,\frac{2}{3}\,u_py_o \tag{62}$$

In physical variables, this flux is $gA\delta_mV_h/kC^2$ which is much smaller than that in the plug flow by a factor δ_m/h.

WAVE DAMPING

Similar to the discussion in MEI and LIU (1987), wave attenuation is contributed by dis-

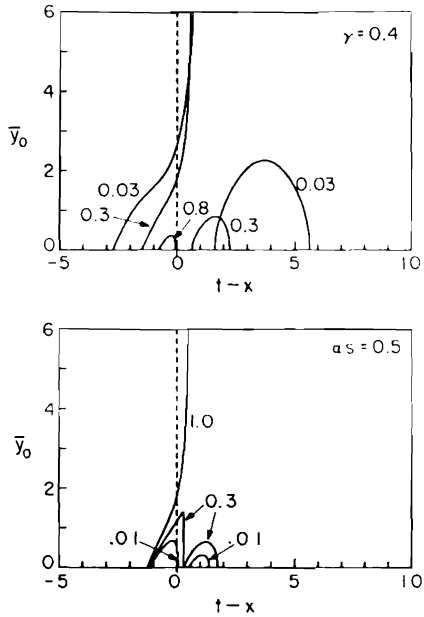

Figure 8. Time variation of shear layer thickness $\bar{y}_o$.
(8.a): $\gamma = 0.4$; $\alpha s = 0.03, 0.3, 0.8$.
(8.b): $\alpha s = 0.5$; $\gamma = 0.01, 0.3, 1.0$.

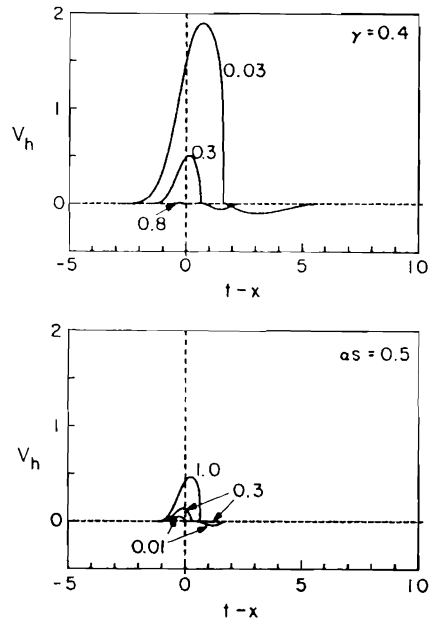

Figure 9. Time variation of mud discharge $\bar{V}_h$ in the shear region.
(9.a): $\gamma = 0.4$; $\alpha s = 0.03, 0.3, 0.8$.
(9.b): $\alpha s = 0.5$; $\gamma = 0.01, 0.3, 1.0$.

sipation in the bottom shear layer, at the yield surface y_o by τ_o, and by the interfacial stress τ_I from water. Since the interfacial stress is allowed to be greater than the yield stress, there can be a shear layer just below the interface. Dissipation in the upper shear layer must in principle be added as well. Formally we have in physical variables

$$\frac{d}{dx} < EC_g > = \frac{d}{dx} < pUH > = -D \qquad (63)$$

where $< >$ represents time integration from $-\infty$ to ∞ and

$$D = D_y + D_m + D_w + D'_y + D'_m \qquad (64)$$

The rate of dissipation from the bottom shear layer is

$$D_y + D_m = < \int_{-h}^{-h+y_0} \left(\tau_0 \, \mathrm{sgn} \frac{\partial u_b}{\partial y} + \mu_m \frac{\partial u_b}{\partial y} \right) dy > \qquad (65)$$

where D_y is the first term due to work done by the yield stress and D_m is the second term due to viscous dissipation. Similarly the dissipation from the shear layer beneath the interface is

$$D'_y + D'_m = \tau_0 < |u_I - u_p| > + \mu_m < \int_{-y_0}^{\eta} \left(\frac{\partial u_m}{\partial y} \right)^2 dy > \qquad (66)$$

Since the velocity variation is small, as estimated in (21), contribution from (66) is negligible. For the same reason, the work done by the turbulent interfacial stress is approximated by

$$D_w = \frac{1}{2} f \rho < |U - u_p|^3 > \qquad (67)$$

Using scales at the initial station $x = 0$ which are denoted by the subscript $(\ )_o$, we define the normalized variables

$$\tilde{A} = A(x)/A_0 \quad \tilde{H} = H(x)/\tilde{H}_0 \text{ and } \tilde{x} = k_0 x \qquad (68)$$

Equation (63) then becomes

$$\frac{d}{d\tilde{x}}(\tilde{A}\tilde{H})^{3/2} = -\frac{\sqrt{3}}{4} \frac{h}{H_0} \frac{\tilde{A}^2}{\tilde{H}} \left(\frac{1}{3} F_1 + \frac{2}{3\sqrt{3}} \frac{\delta m}{h} F_2 + \frac{f}{h} \sqrt{A_0 H_0} \sqrt{\tilde{A}\tilde{H}} \, F_3 \right) \qquad (69)$$

where

$$F_1 = 4\int_{-\infty}^{\infty} u_p d\sigma \tag{70}$$

$$F_2 = 2\int_{-\infty}^{\infty} \frac{(u_p s)^2}{y_0} d\sigma \tag{71}$$

$$F_3 = \int_{-\infty}^{\infty} |U - u_p|^3 d\sigma \tag{72}$$

The effect of the yield stress F_1 is plotted in dashed lines in Figure 10 vs αs which measures the yield stress, for $\gamma = 0.0, 0.5$ and 1.0, which measures the interfacial friction. As γ increases the plug flow is prolonged in time, resulting in greater work done by the yield stress F_1. F_1 is small for both small αs and large αs, the latter because mud no longer moves. The effect of viscous dissipation F_2 increases with γ also, due to the increases in u_p, as shown by decreasing solid lines in Figure 10. On the other hand, for given αs, u_p increases with γ. The increase of u_p leads to the reduction of $U - u_p$ and the dissipation by the interfacial stress F_3 increases (see increasing solid lines in Figure 10). As discussed in Section 3, mud ceases to move when $\alpha s > (\alpha s)_c$. Then $u_p = 0$ which implies that $F_1 = F_2 = 0$ and from (72) $F_3 = 16/15$. This corresponds to the constant maximum shown in Figure 10.

The information on F_1,F_2 and F_3 is first applied to a sea bed with horizontal bottom and constant mud depth. The inputs at $x = 0$ are:

$$\frac{h}{H} = 0.1, \frac{\delta m}{h} = 0.02,$$

$$\frac{1}{h}\sqrt{A_0 H}e = 1.0,$$

$$Re' = 4 \times 10^4$$

$$(\alpha s)_0 = 0.01, 0.1, 0.3, 0.6, 0.8$$

where the subscript o marks the value at the starting point. For $(\alpha s)_0 = 0.01$, 0.6 and 0.8 the effect of F_1 is weak but for $(\alpha s)_0 = 0.1$ and 0.3, F_1 is significant.

The results are shown in Figure 11 with solid lines for continuous mud motion, long dashed lines for intermittent motion and short dashed lines for stationary mud layer. For comparison, the result for a smooth stationary bed with $f = 0.01$ is plotted in short dashed line. As can be seen, even for $(\alpha s)_0 = 0.01$, the damping effect

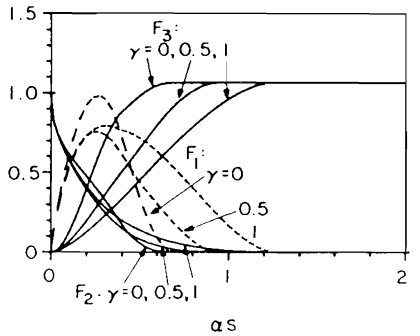

Figure 10. Variation of F_1 (dashed lines), F_2 and F_3 vs αs for $\gamma = 0.0, 0.5, 1.0$.

from a moving mud layer is strong than that from a stionary sea bed. In these curves we mark by circles the start of intermittent mud motion and by crosses the restart of continuous mud motion. The asterisk indicates the point where mud layer ceases to move. Referring back to Figure 6.a, we find $f \approx 0.06$ for $Re_o' = 4 \times 10^4$ and $(\alpha s)_o = 0.01$. Thus in (69), the coefficient in front of both F_2 and F_3 are of the order 10^{-2}. The dominant effect comes from F_1, the yield stress. Hence the rate of dissipation depends largely on the value of F_1. From Figure 10, $(\alpha s)_o = 0.01$, 0.6 or 0.8 gives very small value of F_1 compared to the case $(\alpha s)_o = 0.1$ and 0.3. This is why the result for $(\alpha s)_o = 0.1$ and 0.3 shows stronger damping.

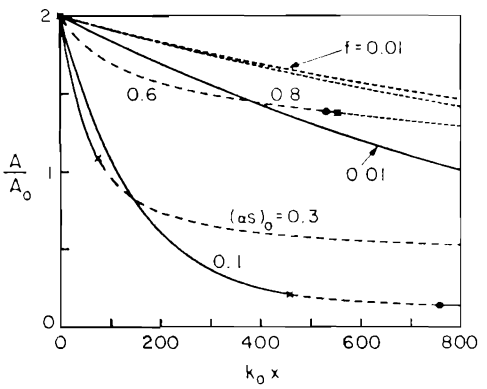

Figure 11. Dimensionless wave amplitude vs fetch on a horizontal bed. The inputs at the starting point are $h/H = 0.1$, $\delta_m/h = 0.02$, $\sqrt{AH}/h = 1.0$, $Re' = 4 \times 10^4$, $\alpha s = 0.01$, 0.1, 0.3, 0.6, 0.8. The curve marked $f = 0.01$ is computed for a stationary bed.

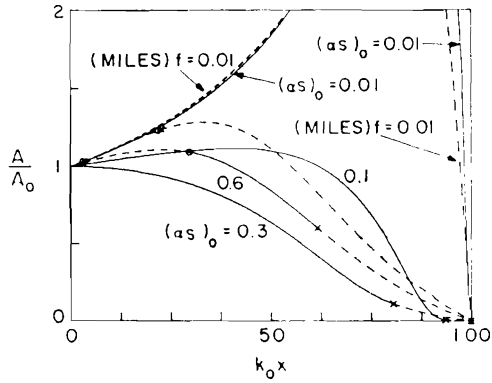

Figure 12. Dimensionless wave amplitude vs fetch on a sloping bed. The inputs at the starting point are h/H_0 = 0.1, δ_m/h = 0.02, $\sqrt{A_0H_0}/h$ = 1.0, $Re'_0 = 4 \times 10^4$, s = 0.001, $(\alpha s)_0$ = 0.01, 0.1, 0.3, 0.6, 0.8. The curve marked f = 0.01 is computed according to MILES (1983).

As wave amplitude decreases, the yield stress becomes stronger with respect to wave forcing. αs increases in accordance with (42) along the fetch. From Figure 6.a, for $Re' = 4 \times 10^4$, we find f to be a constant $\cong 0.015$ for $\alpha s \geq 0.1$. For the case $(\alpha s)_0 = 0.01$, f is also approximately a constant $\cong 0.06$ due to the small change in wave amplitude. For $(\alpha s)_0 = 0.8$, the mud no longer moves, hence the damped wave amplitude is almost the same as that of a rigid smooth bed with f = 0.01.

The information on the three local dissipation rates is next applied to a plane beach of mild slope with a mud layer of constant depth. At t = 0 the peak of the solitary wave is at the water depth H_0 and wave amplitude is A_0. The inputs are:

$$\begin{aligned} S &= 0.001, \\ k_0H_0 &= 0.1, \\ Re' &= 4 \times 10^4, \\ h/H_0 &= 0.1, \\ \delta_m/h &= 0.02, \\ \frac{1}{h}(A_0H_0)^{1/2} &= 1.0, \\ (\alpha s)_0 &= 0.01, 0.1, 0.3, 0.6, 0.8 \end{aligned}$$

Typical physical magnitudes can be: h = 1 m, H_0 = 10 m, A_0 = 0.1 m. For S = 0.001, the shoreline is at $k_0x = 100$. The amplitude ratio $A(x)/A_0$ is integrated from (69) as a function of the dimensionless fetch k_0x. In Figure 12 the effects of the initial $(\alpha s)_0$ are shown. Because of shoaling, the wave amplitude increases first for almost all cases. As wave amplitude increases, αs decreases and F_1 increases. Eventually, the yield stress effect overcomes shoaling and the wave amplitude begins to decrease, hence αs increases. The computed friction factor is approximately $f \cong 0.02$ throughout. As the waves travel towards the shore, there is always intermittent mud motion near the shore. The mud motion stops at the shore where the wave amplitude goes to zero. For comparison, the wave damping curve for a stationary bottom and a constant friction factor f = 0.01 is computed from the theory of MILES (1983) and is shown as the highest dashed line.

CONCLUSIONS

As an improvement over an earlier paper we have studied the role of interfacial friction on the motion of a cohesive mud layer under a solitary wave. The mud is modeled as a Bingham plastic fluid. To this end it is necessary to modify the empirical law of friction factor in order to account for possible motion of the muddy bottom. As a consequence the friction factor must be found as a part of the solution. In the event of mud motion, the relative velocity between water and mud decreases and the friction factor may increase as compared to a smooth but stationary bottom, although the interfacial stress actually decreases. This is consistent with the findings of MAA (1986). Mass transport and the rate of wave damping are also strongly affected by the interfacial friction.

A major assumption made here is that the mud layer is much thinner than the water layer above. This renders the interfacial waves unimportant. Removal of this and other restrictions deserve to be pursued for a cohesive mud bottom.

ACKNOWLEDGMENTS

We thank the Office of Naval Research, Ocean Engineering Program for financial support through Contract No. 00014–83–K–0550.

LITERATURE CITED

ALLERSMA, E., 1982. Mud in estuaries and along coasts. *International Symposium on River Sedimentation*, Beijing, China.

ARIATHURAI, R. and ARULANANDAN, K., 1978. Erosion rates of cohesive soils. *Journal of Hydraulics Division, Proceedings of the ASCE*. 104, HY2, 279-283.

DIXIT, J.G.; MEHTA, A.J., and PARTHENIADES, E., 1982. Redepositional properties of cohesive sediments deposited in a long flume. *UFL/COEL*—82/DO2, U. of Florida, Gainesville.

MAA, P.Y., 1986. Erosion of soft muds by waves. PhD Dissertation, University of Florida, Gainesville.

MAA, P.Y. and MEHTA, A.J., 1987. Mud erosion by waves: a laboratory study. *Continental Shelf Research*. 7 (11/12), 1269-1284.

MEI, C.C. and LIU, K.F., 1987. A Bingham plastic model for a muddy sea bed under long waves. *J. Geophy. Res. (Oceans)*. 92 (C13), 14581-14594.

MILES, J.W., 1983. Solitary wave evolution over a gradual slope with turbulent friction. *Journal of Physical Oceanography*. 13, 551-553.

PARCHURE, T.M. and MEHTA, A.J., 1985. Erosion of soft sediment deposit. *Journal of Hydraulic Engineering, Proceedings. ASCE*, 111, 1982 (10), 1308-1326.

SCHUCKMAN, B. and YAMAMOTO, T., 1982. Nonlinear mechanics of sea—bed interactions. Part II—Wave tank experiments on water wave damping by motion of clay beds. *Technical Report* TR 82-1. Rosenstiel School of Marine and Atmospheric Science, University of Miami, Miami, Florida, 132 pp.

TUBMAN, M. W. and SUHAYDA, J. N., 1976. Wave action and bottom movements in fine sediment. *Proceedings of the 15th Coastal Engineering Conference*. 2, 1168-1183. ASCE, New York.

VAN RIJN, L.C., 1985. The Effect of Waves on Kaolin/Sand Beds. Delft Hydraulic Lab. *Report on Model Investigation* M2060 Aug.

WAN, Z.H., 1982. Bed material movement in hyperconcentrated flow. Technical University of Denmark. *Series paper* No. 31, Institute of Hydrodynamics and Hydraulic Engineering.

□ ZUSAMMENFASSUNG □

Küstennaher Schlick und Schlick am Boden von Ästuaren enthält einen hohen Anteil von Tonpartikeln. Die Rheologie dieses kohäsiven Materials ist sehr komplex und es bestehen sehr unterschiedliche Modelle zur Vorhersage der wechselseitigen Beinflussung von Schlick und Wellen. In diesem Aufsatz konzentrieren wir uns auf das "Bingham-plastic"-Verhalten, welches bekanntermaßen in Ästuar- und Flußschlick mit hoher Tonkonzentration existiert. Unter berücksichtigung der Reibung zwischen den verschiedenen Schichten, wird die Bewegung in einer dünnen Schlickschicht untersucht. Diese Bewegung wurde induziert durch eine einzelne Welle, die sich in einer sehr viel mächtigeren überlagernden Wasserschicht ausbreitet. Die Auswirkungen der Schlickbewegung auf die Verminderung der Wellenbewegung wird für horizontale und geneigte Meeresböden berechnet.—*Ulrich Radtke, Geographisches Institut, Universität Düsseldorf, F. R. G.*

□ RÉSUMÉ □

La vase molle recouvrant le fond de certains estuaires et littoraux a une forte concentration en particules argileuses. Les propriétés rhéologiques de ce matériau cohésif sont très complexes et il y a eu des modèles bien différents pour prédire les effets mutuels des vases et des vagues. Ce papier insiste sur le comportement "de Bingham" que l'on sait exister dans certains estuaires et rivières à forte concentration. Analyse à l'intérieur d'une fine couche d'argile le mouvement induit par une onde solitaire se propageant dans une couche d'eau plus épaisse, ce en incluant la friction interne. Les effets du déplacement de la vase sur l'amortissement des vagues sont calculés pour un fond marin horizontal et pour un fond en pente.—*Catherine Bressolier, Laboratoire de Géomorphologie EPHE, Montrouge, France.*

□ RESUMEN □

El lodo encontrado en el fondo de algunos estuarios y costas contiene una alta concentración de particulas arcillosas. Las propiedades reológicas de este material cohesivo son muy complejas y se ha desarrollado numerosos modelos para la predicción de la interacción oleaje-lodo. Este articulo se centra en el comportaminento Bingham-plástico que se conoce existe en los lodos de estuarios y rios. Incluyendo una fricción interfacial, se analiza el movimiento en una capa fina de lodo inducido por una onda solitaria propagándose en una capa mucho mayor de agua sobre el lodo. Se calcula, además, la reducción de la onda debida al movimiento del lodo tanto en fondo horizontal como en fondo inclinado.—*Department of Water Sciences, University of Cantabria, Santander, Spain.*